Open access • Journal Article • DOI:10.1103/PHYSREVB.90.085147

Trapping and detrapping in SrAl 2 O 4 : Eu , Dy persistent phosphors: Influence of excitation wavelength and temperature — Source link

Jonas Botterman, Jonas Joos, Philippe Smet

Institutions: Ghent University

Published on: 28 Aug 2014 - Physical Review B (American Physical Society)

Trapping and detrapping in $SrAl_2O_4$:Eu,Dy persistent phosphors: Influence of excitation wavelength and temperature

Jonas Botterman,* Jonas J. Joos,* and Philippe F. Smet†
LumiLab, Department of Solid State Sciences, Ghent University, Krijgslaan 281-S1, 9000 Gent, Belgium
and Center for Nano- and Biophotonics, Ghent University, Sint-Pietersnieuwstraat 41, 9000 Gent, Belgium
(Received 12 June 2014; published 28 August 2014)

$SrAl_2O_4$:Eu,Dy is presumably the best known persistent luminescent phosphor. At room temperature, its green emission remains visible for hours after switching off the excitation. It is known that upon lowering the temperature of the phosphor a second photoluminescence emission band arises in the blue part of the visible spectrum, although its origin is still the subject of discussion. In this paper we thoroughly study the origin of both emission bands in $SrAl_2O_4$:Eu,Dy and we attribute this to europium ions substituting for the two different Sr sites in the phosphor's monoclinic host lattice. The photoluminescence properties, the thermal quenching behavior, and photoluminescence lifetime of both emission bands are investigated. A lanthanide energy level scheme is constructed for both sites. Using an integrated approach, i.e., combining charging, afterglow, and thermoluminescence measurements in the same run, we study the charging or trap filling processes in $SrAl_2O_4$:Eu,Dy upon excitation with site selective excitation wavelengths and at different temperatures. We show that trap filling is a thermally activated process when the green emitting center is excited at 435 nm. Furthermore, we also demonstrate that the distribution of filled traps after charging depends strongly on the excitation wavelength and thus on which Eu^{2+} center has been excited. This suggests trapping of the electron close to the ionized Eu^{2+} ion, without full delocalization to the conduction band during the trapping process. Finally, the quantum efficiency of the persistent luminescence is estimated at 65 (+/−10)%.

DOI: 10.1103/PhysRevB.90.085147 PACS number(s): 78.60.Kn, 78.55.Hx, 78.55.−m, 72.20.Jv

I. INTRODUCTION

The discovery of europium and dysprosium codoped strontium aluminate ($SrAl_2O_4$:Eu,Dy) in 1994 marked the beginning of the second generation of persistent or afterglow phosphors, also called glow-in-the-dark materials [1–3]. Although many new persistent phosphors have been reported since then [1,4], rare earth doped strontium aluminates are still by far the most studied and commercialized compounds. $SrAl_2O_4$:Eu,Dy is widely used in various glow-in-the-dark applications, ranging from emergency signage and watch dials to toys. Besides commercial applications, persistent luminescent phosphors—including $SrAl_2O_4$:Eu,Dy—have also been demonstrated to be useful for in vivo imaging [5–7]. Another peculiar phenomenon in this compound is mechanoluminescence. This type of luminescence is closely related to persistent luminescence and has been studied intensively in the framework of pressure sensing [8–12].

At room temperature, $SrAl_2O_4$:Eu shows a characteristic Eu^{2+} based broad emission band with a maximum at 520 nm and a FWHM of about 85 nm. The addition of Dy^{3+} does not alter the emission spectrum, but considerably enhances the persistent luminescence intensity [2]. At room temperature, the afterglow of $SrAl_2O_4$:Eu,Dy lasts for several hours, which is the result of the gradual, thermally assisted release of trapped charges in the phosphor. This long afterglow is in contrast to the duration of only a few minutes for the variant without codopant [13]. Even longer afterglow durations can be obtained by tuning the synthesis conditions, e.g., by boron addition [14].

Although the persistent luminescent material $SrAl_2O_4$:Eu,Dy has been described about 20 years ago, the details of the mechanism of this state-of-the-art persistent phosphor are still not fully clear. Detailed knowledge of the underlying mechanism of persistent luminescence is lacking, more specifically on the trapping and detrapping processes. First of all, it is still unclear whether the traps are related to host defects, the trivalent codopant, or a combination of both [15–17]. Different opinions also exist on the trapping and detrapping routes, regarding the role of the conduction band and whether tunneling processes also play a role [18,19]. Although several research approaches are available to study the trapping and detrapping processes, the reports in literature commonly consider only one or two of the following aspects of the trapping process in sufficient detail. When exciting a persistent phosphor, one observes that the luminescence intensity does not immediately reach a constant value (the so-called "charging behavior"). Secondly, after ending the excitation of the phosphor, the emission intensity slowly decreases (the "afterglow"). Thirdly, the thermoluminescence (TL) spectrum allows one to study persistent phosphors in a reasonable time frame, by monitoring the emission as a function of increasing temperature for a charged phosphor. Nevertheless, all three processes are intimately connected by the same underlying trapping and detrapping processes. When devising a model, it should simultaneously take all three processes into account.

Therefore we designed a dedicated experiment that combines a charging, an afterglow, and a TL measurement. This experiment was subsequently performed at different temperatures, ranging from 193 to 353 K. Note that the afterglow behavior is normally studied at room temperature only. The significant release of charges from traps at this temperature, however, unnecessarily complicates matters, which incited us

*These authors contributed equally.
†Corresponding author: philippe.smet@ugent.be

to perform these experiments also below room temperature. It turns out that these integrated experiments provide valuable information on the trapping and detrapping processes in persistent phosphors, and are here performed on the model phosphor $SrAl_2O_4$:Eu,Dy. Finally, it became clear that the energy levels associated to an additional blue emission band, which is fully thermally quenched at room temperature, are playing an important role as well.

In addition to a better understanding of the trapping and detrapping processes in this specific strontium aluminate phosphor, the approach used in this paper is easily transferable to other persistent phosphors, where an integrated charging-afterglow-TL experiment would also allow a better quantitative discussion.

Studying the role of the excitation wavelength on the trapping efficiency is also important from an application's point of view, especially for indoor applications such as safety signage, as the shift from fluorescent lighting to light-emitting diode (LED) based lighting also changes the range of available wavelengths to induce the persistent luminescence. For outdoor applications, e.g., in road signage, a much larger fraction of (near)ultraviolet light is available in the solar spectrum. For bioimaging based on red or infrared emitting persistent phosphors, the required excitation wavelength can be even longer [20]. Therefore the composition and evaluation of persistent phosphors should consider explicitly the role of the excitation wavelength on the trap filling, appropriate for the type of application.

It was recently proposed that afterglow phosphors can be used to fill the dead time in ac-driven light-emitting diodes, to reduce flickering [21,22]. In that respect it is important to notice that under steady state excitation of a persistent phosphor, a large fraction of the light emission during excitation consists of afterglow emission, involving continuous trapping and detrapping. This can potentially lower the overall quantum efficiency of the phosphor, as not every trapped charge carrier eventually leads to an emitted photon. An approach to evaluate the quantum efficiency of this process is proposed in this work.

II. EXPERIMENT

The crystal structure of the studied $SrAl_2O_4$:Eu,Dy powders (GloTech Intl.) was verified by θ-2θ x-ray diffraction (XRD) measurements (Siemens D5000, Cu $K\alpha$ radiation). The measured XRD pattern (not shown) matches the structure of the $SrAl_2O_4$ host lattice (ICSD No. 26466) [23], without traces of other crystalline phases. The substitution of a small amount of Sr atoms by Eu or Dy atoms in the crystal lattice does not have a detectable influence on the XRD spectra and thus we assume that at least for low doping concentration the crystal structure is unaltered.

Photoluminescence (PL) excitation and emission spectra were recorded with a steady state fluorescence spectrometer (Edinburgh Instruments FS920). The thermal quenching measurements on $SrAl_2O_4$:Eu,Dy were conducted using the above-mentioned fluorescence spectrometer combined with a cryostat (Oxford Instruments Optistat CF) in which the sample was heated following a linear temperature profile from 70 to 470 K at a rate of 2 K/min. The sample was excited prior

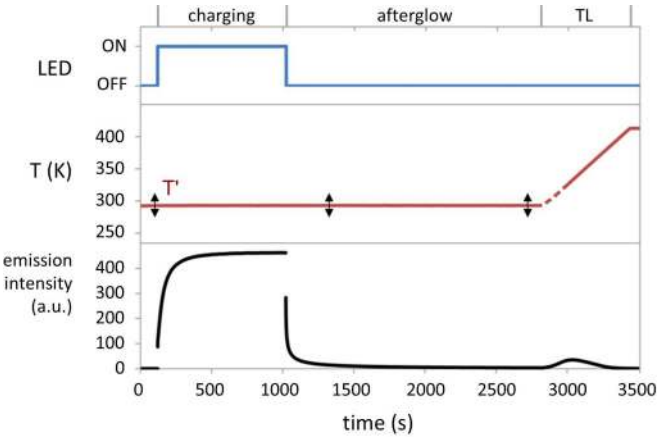

FIG. 1. (Color online) Experiment outline: At a certain temperature T' the $SrAl_2O_4$:Eu,Dy sample is excited for 15 min using a 370 nm LED. After the LED is switched off the afterglow emission is recorded for 30 min, also at temperature T'. Subsequently, the sample is heated linearly from temperature T' up to 420 K at 0.2 K/s while continuously measuring the luminescent emission. T' can be varied in the range from 193 K up to 353 K.

to and during the measurement using a 370 nm LED with high intensity ($I_{LED} = 20$ mA), to limit temporary effects of trapping and detrapping on the luminescence intensity. An emission spectrum was recorded every 1.5 minutes (i.e., every 3 K).

Temperature-dependent luminescence lifetimes were measured using a pulsed nitrogen laser (repetition frequency of 1 Hz) as an excitation source ($\lambda = 337$ nm), an intensified CCD (Andor iStar) attached to a Jarrel-Ash monochromator, and the above-mentioned cryostat to control the sample temperature. Given that considerable afterglow emission is present at elevated temperatures, "luminescence lifetime" refers to the decay in the emission intensity within a short time after the pulsed excitation (i.e., within a few microseconds).

In order to investigate the temperature dependency of the charging and afterglow behavior of the phosphor, the following experiment was conducted (Fig. 1): At a certain temperature T' a pressed pellet of $SrAl_2O_4$:Eu,Dy powder is charged using a constant illumination intensity. Subsequently, the light source is switched off, and the afterglow is recorded for 30 min at the same temperature T', immediately followed by a TL glow curve measurement, starting at T'. A series of these combined experiments was performed, each one having a different temperature T' for charging and afterglow. Before each combined experiment the sample was heated to assure that all relevant traps were empty at the start of each experiment.

These experiments were performed using a home-built setup. The cooling and heating stage, built into a small vacuum chamber, enables charging and afterglow measurements at temperatures in the range from 193 to 353 K and thermoluminescence glow curve measurements up to 420 K at a heating rate of 0.2 K/s. The light emitted from the phosphor during charging, afterglow, and TL measurement was collected and guided by an optical fiber to a ProEM1600 EMCCD camera attached to an Acton SP2300 monochromator (Princeton Instruments). During the entire experiment, a full emission

spectrum was measured every 0.5 s, enabling investigation of both spectral shape and intensity of the emission during the entire experiment. The excitation source for the charging was a near-UV LED (peaking at 370 nm), which allowed sufficient spectral separation between the emission of the phosphor and the excitation light, or an indigo LED (peaking at 435 nm). A long excitation duration of 15 min was chosen to assure "full" charging of the phosphor.

III. RESULTS

A. Photoluminescence of $SrAl_2O_4$:Eu,Dy

At room temperature and upon excitation at 370 nm, the PL emission of $SrAl_2O_4$:Eu,Dy (Fig. 2) consists of a single broad green emission band. Its peak position (λ_{max} = 521 nm) and bandwidth (FWHM = 80 nm) are in line with literature reports [24,25]. This emission is characteristic for $5d$-$4f$ transitions in divalent europium. Upon lowering the temperature a second, blue, emission band becomes visible (λ_{max} = 445 nm). Although less well studied as the green emission band, its presence has been reported earlier in several papers [16,17,26]. In the figure, the temperature dependency of both blue and green emission upon excitation with 370 nm is visible. The intensity of the blue emission band decreases quickly upon increasing temperature and vanishes at temperatures around 275 K, leaving only the green emission band at higher temperatures.

Figure 3 shows the PL emission and excitation spectra of $SrAl_2O_4$:Eu,Dy at 10 K. In the emission spectrum (solid line, λ_{ex} = 370 nm) both blue and green emission bands are visible (λ_{max} = 445 nm, FWHM = 35 nm; and λ_{max} = 524 nm, FWHM = 60 nm, respectively). As the green and blue emission bands are hardly overlapping, it is possible to measure the PL excitation spectrum for both emission bands separately. The PL excitation spectrum for the blue emission band (λ_{em} = 445 nm) extends from 250 nm up to 420 nm, while the PL excitation spectrum for the green emission band (λ_{em} = 520 nm) ranges from 250 nm up to 460 nm. Consequently, excitation with wavelengths shorter than 420 nm yields the blue and green emission bands simultaneously.

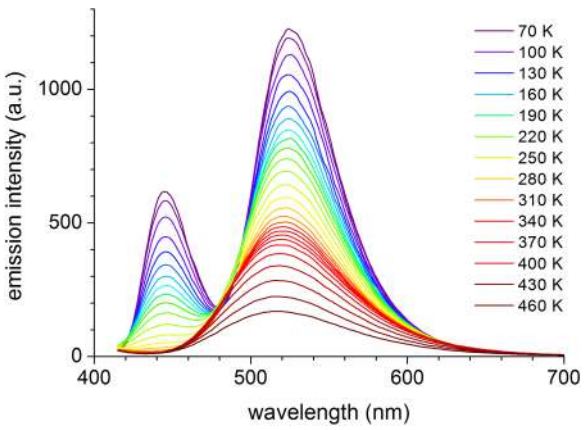

FIG. 2. (Color online) Emission spectra (λ_{ex} = 370 nm) of $SrAl_2O_4$:Eu,Dy at different temperatures ranging from 70 K up to 460 K in steps of 15 K.

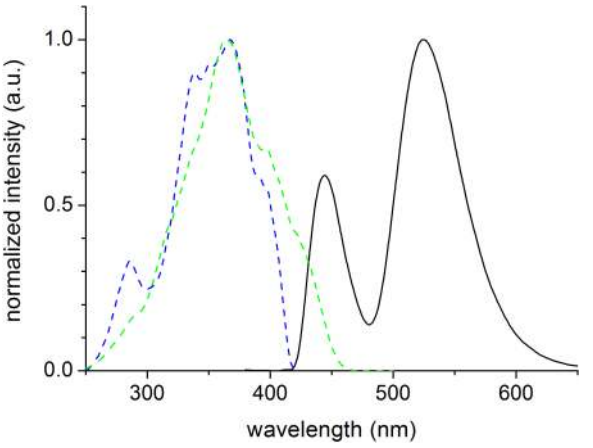

FIG. 3. (Color online) Emission spectrum (solid line, λ_{ex} = 370 nm) and excitation spectra (blue dotted line, λ_{em} = 445 nm and green dashed line, λ_{em} = 520 nm) of $SrAl_2O_4$:Eu,Dy at 10 K.

B. Luminescence lifetime and thermal quenching of $SrAl_2O_4$:Eu,Dy

Figure 4(a) shows the correlation between the thermal quenching and the luminescence lifetime of the blue emission band of $SrAl_2O_4$:Eu,Dy. The thermal quenching curve is constructed by plotting the integrated blue emission as a function of temperature. The blue emission shows the first signs of thermal quenching at a temperature around 80 K and is completely quenched around 275 K, as could also be observed in Fig. 2. The luminescence lifetime of the blue emission is 380 ns at low temperature, and starts to decrease when thermal quenching sets in at 80 K. Although the decay then becomes multiexponential (not shown), the lifetime of the main component decreases more or less along the thermal quenching profile [Fig. 4(a)].

Figure 4(b) shows the temperature dependence of the emission intensity of the green emission band upon excitation with 370 nm (main figure) and 435 nm (inset). Upon excitation with 370 nm the emission intensity starts to decrease from temperatures around 80 K, similar to the quenching of the blue emission band; however, complete quenching of the green emission only occurs at temperatures above 450 K. The thermal quenching profile is rather unconventional, with three partial drops in the emission intensity (at around 80, 220, and 400 K). These three partial drops were also observed when measuring the thermal dependence in the opposite direction, i.e., by going from high to low temperature, so that artificial effects related to afterglow or trap filling can be ruled out. Upon excitation with 435 nm [inset of Fig. 4(b)] the green emission remains nearly constant in the temperature range from 70 to 220 K (i.e., without the first drop observed at 80 K, as in the case of excitation at 370 nm), then shows a drop in intensity but only quenches completely for temperatures presumably higher than 500 K.

Figure 4(b) also shows the luminescence lifetime of the green emission band upon excitation with 337 nm. At low

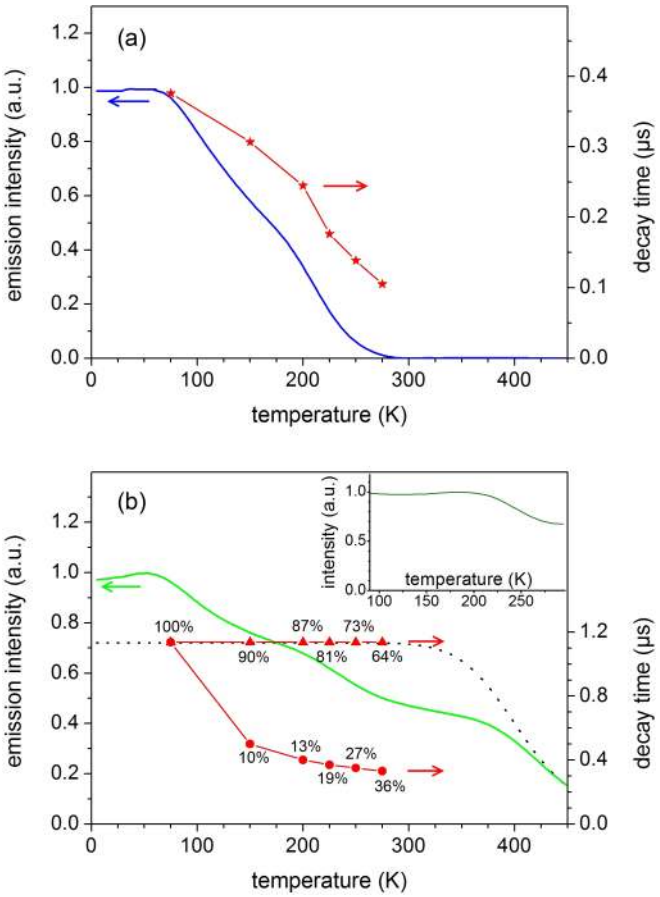

FIG. 4. (Color online) (a) Temperature dependence of the emission intensity of the blue emission band in $SrAl_2O_4$:Eu,Dy (λ_{ex} = 370 nm) combined with the luminescence lifetime of the blue emission band at various temperatures (red stars). (b) Temperature dependence of the emission intensity of the green emission band in $SrAl_2O_4$:Eu,Dy upon excitation with 370 (green line) or 435 nm (inset). Lifetime values for the green emission band are indicated by red symbols at various temperatures. The percentages in the figure indicate the fractions in the total emission intensity assigned to the slow (red triangles) and the fast (red dots) component. The black dotted line is discussed in the text.

temperatures (<100 K) the decay profile can be fitted with a single exponential with a lifetime of 1140 ns. At higher temperatures, a deviation from the single exponential decay is observed with the emergence of a faster decay component while the 1140 ns component is still preserved. To quantify the effect, the decay profiles were fitted with two exponentially decaying components, obeying

$$I(t) = I_1 e^{-t/\tau_1} + I_2 e^{-t/\tau_2}.$$

The fraction in the total emission intensity assigned to component τ_i can then be calculated as

$$f_i = \frac{\int I_i e^{-t/\tau_i} dt}{\int I(t) dt} = \frac{I_i \tau_i}{I_1 \tau_1 + I_2 \tau_2} \quad (i = 1,2).$$

The fraction in the total emission intensity assigned to each component is indicated as a percentage in Fig. 4(b). At higher temperature, the lifetime for the fast component shortens, combined with an increase in the fraction it represents in the total emission.

C. Charging, afterglow, and TL combined experiment on $SrAl_2O_4$:Eu,Dy

Figures 5(a)–5(c) show the results of the combined experiment as described in the experimental section (Fig. 1) using the 370 nm LED as excitation source. The color codes in all three individual figures are the same. Figure 5(a) shows the charging curves, i.e., the integrated emission intensity as a function of time, at different temperatures. The different curves are plotted with respect to the same vertical axis without being displaced. Figure 5(b) shows the afterglow curves measured at different temperatures plotted in a semilogarithmic graph for better visibility. Figure 5(c) shows the measured TL glow curves, immediately started after the 30 min of afterglow measurement.

In Fig. 5(b) the temperature dependence of the afterglow emission of $SrAl_2O_4$:Eu,Dy is clearly visible. The initial afterglow intensity is highest for the higher temperatures as more thermal energy is then readily available to release electrons from traps. A side effect is a faster decay, derived from the steepness of the afterglow curves, because of a faster emptying of the filled traps. At low temperature, the thermal energy is not sufficient to efficiently release trapped electrons and hardly any afterglow emission is observed at temperatures below 243 K. Only during a very short period immediately after the excitation a weak afterglow signal is measured at these temperatures, which might be the result of the release of electrons from a limited number of very shallow trap levels.

From the TL glow curves in Fig. 5(c) one can see that multiple trap levels or a distribution of trap levels are present in $SrAl_2O_4$:Eu,Dy. When measuring a TL glow curve starting at temperatures below 250 K the glow curves peak around 310 K and a prominent shoulder at the low-temperature side of the glow curve (around 275 K) can be seen. Upon charging at higher temperatures the peak shifts to higher temperatures.

Figure 6 shows for every combined experiment (i.e., at every temperature) the accumulated light emission during the 30 min afterglow (blue dots) and during the TL measurement (red triangles). The black diamonds in the figure show the total accumulated light emission from the phosphor, i.e., the sum of the accumulated light emission during afterglow and TL, and is a measure of the amount of filled traps at the end of the excitation.

The same series of combined experiments were conducted using a 435 nm LED as the excitation source—which excites only the green emission (Fig. 3)—to charge the $SrAl_2O_4$:Eu,Dy sample. The results of this series are shown in Figs. 5(d)–5(f). The figures show large similarities with the results of excitation at 370 nm [Figs. 5(a)–5(c)], although marked differences are visible. In the afterglow curves the initial decay of the afterglow is less steep after charging with 435 nm and at very low temperatures (<243 K) no afterglow at all is measured, not even during a very short period immediately after the excitation as was the case after charging with 370 nm. The TL part shows the most pronounced difference between excitation at 370 and 435 nm. In the latter case, no traps were actually filled during charging when

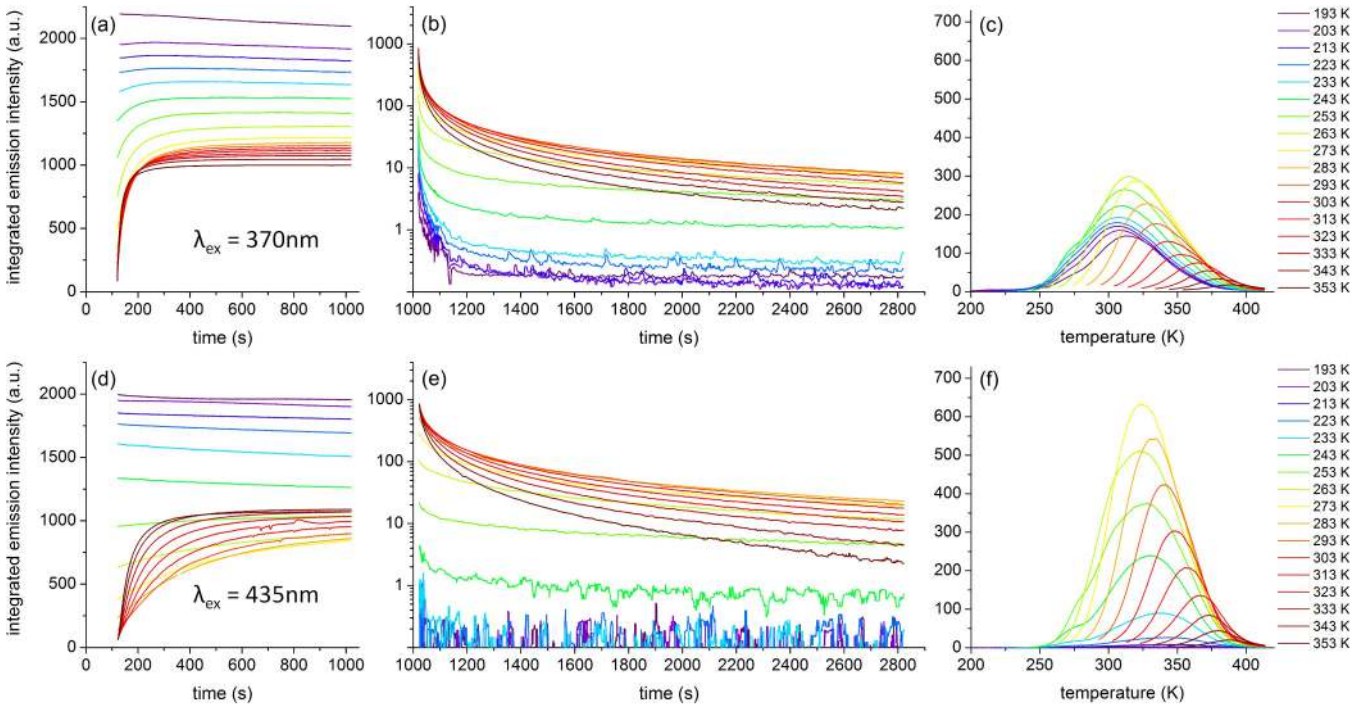

FIG. 5. (Color online) Influence of the temperature in the charging-afterglow-TL sequence on the integrated emission intensity of $SrAl_2O_4$:Eu,Dy, as defined in Fig. 1. (a) Time evolution of the emission intensity upon excitation ($\lambda_{ex} = 370$ nm), started at $t = 120$ s, (b) integrated afterglow intensity at different temperatures after the excitation, and (c) subsequent thermoluminescence glow curves. (d), (e) and (f) are the same as (a), (b), and (c) but with $\lambda_{ex} = 435$ nm. The thermoluminescence glow curves are recorded from the temperature of excitation and afterglow up to 420 K at a heating rate of 0.2 K/s.

temperature was below 220 K, in contrast to the significant TL intensity upon charging with 370 nm at the same temperature. Using the same analysis as for excitation upon 370 nm, the total amount of trapped charges is the sum of the afterglow and the thermoluminescence (Fig. 7).

IV. DISCUSSION

The discussion section of this paper is organized as follows. In Sec. IV A, we first investigate in detail what could be the origin of both emission bands in $SrAl_2O_4$:Eu,Dy, as this is up to now still an open debate. This will be done on the basis of the structure of the excitation spectrum for both emission bands combined with crystallographic information on the phosphor's host lattice. A vacuum referred energy level scheme is derived using the approach presented by Dorenbos, containing the position of the energy levels for the divalent and trivalent energy levels with respect to the host's valence and conduction bands. In Secs. IV B and IV C, we use this energy level scheme to understand the relevant processes for the persistent

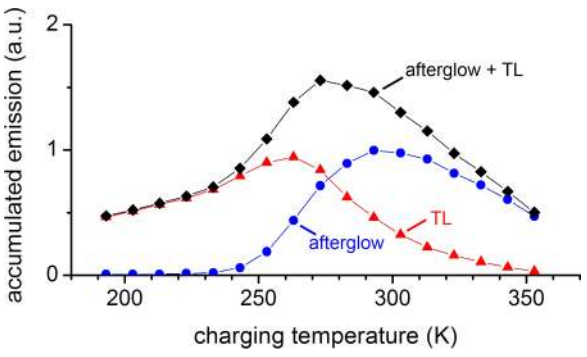

FIG. 6. (Color online) Blue dots: Integrated light emission during the afterglow (measured for 30 min) after charging with 370 nm at different temperatures (Fig. 5). Red triangles: Integrated light emission during the thermoluminescence glow curve measurement. Black diamonds: Sum of afterglow and thermoluminescence, i.e., a measure for the total amount of filled traps at the end of the excitation.

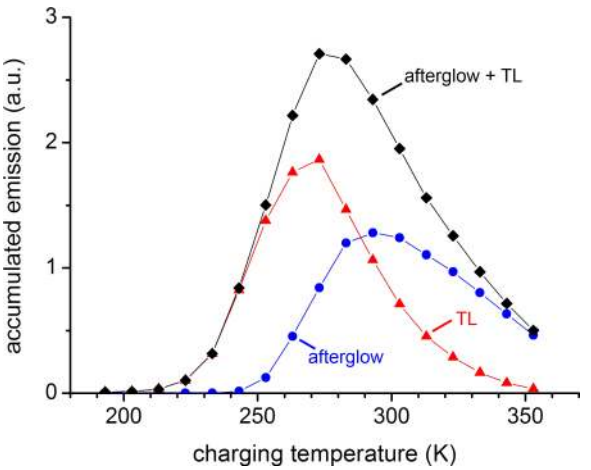

FIG. 7. (Color online) same as Fig. 6, but upon excitation at 435 nm at different temperatures.

luminescence in $SrAl_2O_4$:Eu,Dy, in particular the thermal quenching behavior (Sec. IV B) and the charging or trap filling behavior (Sec. IV C). In Sec. IV D we provide an estimate for the quantum efficiency of the persistent luminescence. The influence of the excitation wavelength during charging on the trap filling is discussed in Sec. IV E. Finally, all results are merged into a mechanism for the trap filling (Sec. IV F).

A. Energy level scheme

1. Previously suggested origins of both emission bands

Different hypotheses concerning the two emission bands in europium doped $SrAl_2O_4$ can be found in literature. Given that there are two nonequivalent strontium sites in the $SrAl_2O_4$ crystal structure, it seems straightforward to assign the occurrence of both emission bands to the substitution of Eu on these two lattice sites. Different coordination for both sites is then expected to sufficiently change the crystal field strength and centroid shift to arrive at the observed spectral differences. Nevertheless, several authors discarded this hypothesis because both sites are seemingly too similar to explain the large energy difference when judging on the emission bands [15,16,18]. As an alternative explanation, Poort *et al.* [26] suggested that the two emission bands result from a possible preferential orientation of the d orbitals of Eu^{2+} on Sr sites that appear to line up. Clabau *et al.* [16] proposed that the blue emission band arises from the charge transfer from the fundamental level of the $4f^7$ configuration of Eu^{2+} to the valence band and is associated to a hole detrapping mechanism. Hölsä *et al.* [27] considered the blue emission band as anomalous low-temperature luminescence and proposed that it originates from a higher Eu^{2+} $5d$ state that may be observed due to the absence of high energy lattice vibrations at low temperatures.

In order to ascertain whether the incorporation of the europium activator on the two similar, but nonequivalent Sr sites can give rise to different luminescent properties and explain the occurrence of the blue and green emission bands in $SrAl_2O_4$:Eu^{2+}, a quantitative approach is followed. As a first step, the crystal structure of $SrAl_2O_4$ is described in Appendix A. Herein, the differences and similarities between the two nonequivalent Sr sites are addressed.

2. Spectroscopic parameters for $SrAl_2O_4$:Eu^{2+}

The low-temperature (10 K) PL emission and excitation spectra of $SrAl_2O_4$:Eu^{2+} were displayed in Fig. 3. The blue ($\lambda_{max} = 445$ nm) and green ($\lambda_{max} = 524$ nm) emission bands give rise to two clearly different excitation spectra. From the shape and position of the excitation spectrum, we can now determine the influence of the local environment on the relevant energy levels of the europium ions, depending on the site.

When the excitation spectra are compared, the most important difference occurs for the spectroscopic redshift, being 1.22 and 1.42 eV for the blue and green emission bands, respectively (Table I). The redshift $D(Eu^{2+}, A)$ in a compound A is the result of two effects: (i) a lowering of the average of the $4f^6 5d$ levels with respect to the location in the free ion [the centroid shift, $\epsilon_c(Eu^{2+}, A)$] and (ii) a splitting of the $4f^6 5d$ levels due to the lowering of the symmetry by the incorporation into the crystal [the crystal field splitting $\epsilon_{cfs}(Eu^{2+}, A)$] [28].

TABLE I. Properties of the emission and excitation spectra of $SrAl_2O_4$:Eu^{2+} (measured at 10 K, all values in eV).

	Green (Sr1)	Blue (Sr2)
Emission maximum	2.37	2.79
FWHM emission band	0.27	0.21
Redshift $D(Eu^{2+}, A)$	1.42	1.22
Crystal field splitting $\epsilon_{cfs}(Eu^{2+}, A)$	1.10	1.13
Centroid shift $\epsilon_c(Eu^{2+}, A)$	1.65	1.44
Stokes shift $\Delta S(Eu^{2+}, A)$	0.43	0.21

In Appendix B, a detailed analysis of the spectroscopic redshifts, associated with the green and blue emission bands is performed in terms of the centroid shift and crystal field splitting. Both quantities are functions of the bond length between the Eu ion and its oxygen nearest neighbors. From this analysis, the different shape of the excitation spectra could be explained based on the differences in bond length of the Sr1 and Sr2 sites. The excitation band of the green emission could be assigned to the Sr1 site, and the excitation band of the blue emission to the Sr2 site. The result of this analysis is summarized in Fig. 8.

3. Stokes shift in $SrAl_2O_4$:Eu^{2+}

What has not yet been explained with this energy level scheme is the striking difference between the Stokes shifts of the two emission bands (Table I). For the blue and green emission centers, values of 0.43 and 0.21 eV are found, respectively. This is the major contribution to the observed difference in emission wavelength between the two bands. Poort *et al.* [26] attribute this difference in Stokes shift to a preferential orientation of a $5d$ orbital on one lattice site, but not on the other, due to interaction with the next nearest neighboring Sr^{2+} ion. This assumption was made not only to explain the difference in Stokes shifts, but also the difference in the low energy offset of the excitation spectra. However, our reasoning above showed that the differences in bond lengths of the nine oxygen ligands are sufficient to explain the difference in excitation spectra. This implies that the difference in Stokes shifts should presumably have another cause than the one proposed by Poort *et al.* [26].

An alternative explanation might be related to differences in the angular charge distribution in the first coordination sphere of the Sr1 and Sr2 sites. For the Sr1 site, a relatively strong asymmetry exists in the charge density, which is not the case for the Sr2 site, where the charge distribution is more homogeneous. This observation hints towards an explanation for the difference in Stokes shift (Table I). If the asymmetry provokes an unbalance for the excited Eu^{2+} dopant on the Sr1 site, the equilibrium position of the ion could shift for the excited state. This yields a bigger Stokes shift for the ion on the Sr1 site (green emission), as can be seen from the parabola in a typical configuration coordinate model. In addition, this should also lead to a larger FWHM of this emission band. This is indeed the case (0.27 eV for the green emission band, which

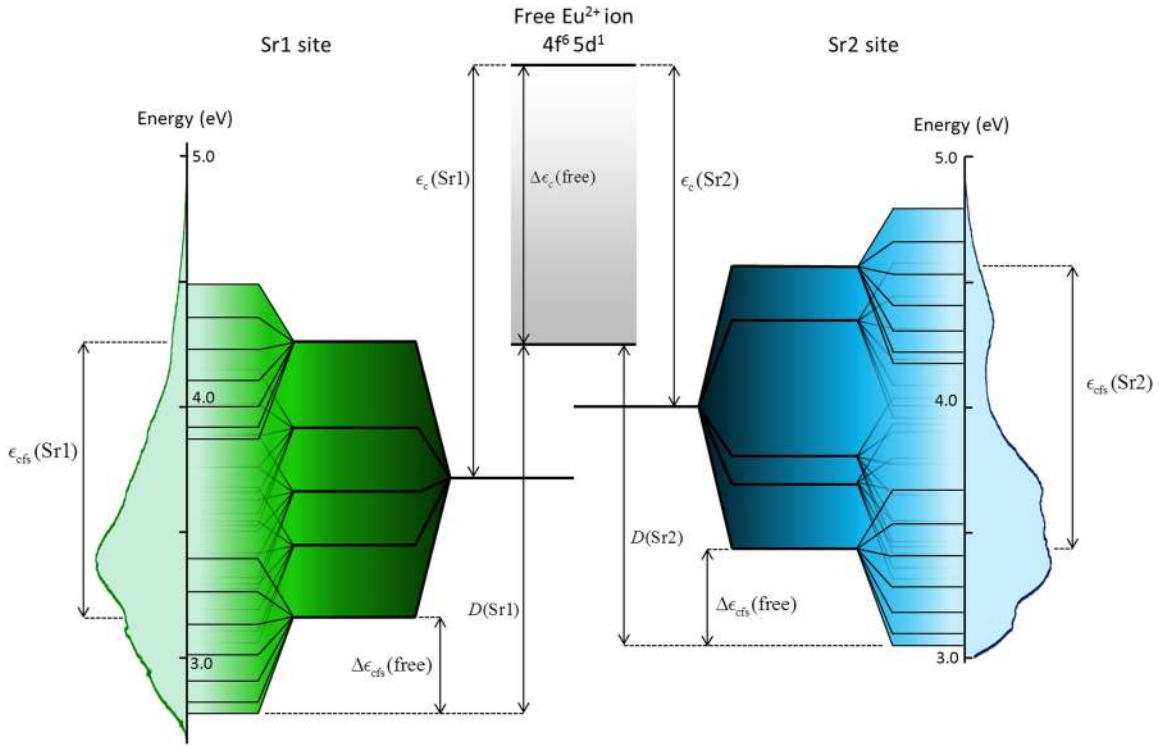

FIG. 8. (Color online) Energy level scheme for Eu^{2+} on the Sr1 (yielding green emission) and on the Sr2 (yielding blue emission) sites in monoclinic $SrAl_2O_4$. The meaning of the different quantities and the connection with the excitation spectra is displayed.

is 29% higher than for the blue emission band; see Table I), providing further proof to the hypothesis.

4. Energy level schemes for lanthanides in $SrAl_2O_4$

At this stage, we have obtained an energy level scheme (Fig. 8) based on a detailed analysis of the spectroscopy of Eu^{2+} in $SrAl_2O_4$. Next, we complete the modeling by positioning the Eu^{2+}-related energy levels with respect to the conduction and valence bands of the host compound. Using Dorenbos' approach, we will also derive the absolute energy level positions of the other rare earth ions in $SrAl_2O_4$, as this proves useful for the discussion of the persistent luminescence of Dy^{3+} codoped $SrAl_2O_4$:Eu^{2+}.

In 2005, an energy level scheme for all the divalent and trivalent lanthanides in $SrAl_2O_4$ was already proposed to explain some characteristics of the persistent luminescent phosphor $SrAl_2O_4$:Eu^{2+},Dy^{3+} [15]. However, in this model, no distinction was made between the two nonequivalent Sr sites where the dopant can reside, nor was sufficiently accurate experimental data available to reliably pin the energy levels. Furthermore, recent developments in the methodology for constructing energy level schemes offer the possibility to obtain more accurate predictions. The details of this calculation, which is done within the framework of the chemical shift model can be consulted in Appendix C. The resulting energy level schemes are shown in Fig. 9. As one can see, different schemes are found for the two sites in the material.

The locations of the $4f^{N-1}5d^1$ excited states for the divalent lanthanide ions are remarkably closer to the bottom of the conduction band than in the energy level scheme, constructed in 2005 [15]. Herein, the $4f^{N-1}5d^1$ levels were rather arbitrarily put to pin the $4f^{13}5d^1$ level of the Yb^{2+} ion at the same height of the bottom of the conduction band, motivated by the fact that this ion shows no luminescence in the $SrAl_2O_4$ host. At present, the chemical shift model offers the possibility to pin the $4f^{N-1}5d^1$ levels in a more accurate way.

For both sites, the ground state for Eu^{2+} is situated less than 1 eV above the middle of the band gap, which leads to an expected divalent valence state for europium when incorporated in $SrAl_2O_4$ [29]. However, from experimental evidence it is clear that sufficiently reducing preparation conditions have to be used to stabilize the divalent state, and that the occurrence of both valence states is not uncommon [30]. For both sites, the Eu^{2+} ground states are at more or less the same energy, which is in line with the chemical shift model. The main difference occurs for the position of the 5*d* level, which is much closer to the conduction band for the blue emission center than for the green emission center. Therefore we expect a much lower thermal quenching temperature for the blue emission center. Note that the positions of the 5*d* levels were derived without making use of the thermal quenching behavior *a priori*.

B. Thermal quenching behavior

As can be seen in Figs. 4(a) and 4(b) there is a clear difference in thermal quenching behavior between the blue and the green emission band. The blue emission is fully quenched at 275 K, while the full quenching for the green emission only occurs at temperatures well above 450 K. This is in correspondence with the constructed energy level scheme (Fig. 9). Hence, as the probable mechanism for thermal quenching is ionization (or, in other words, thermal excitation

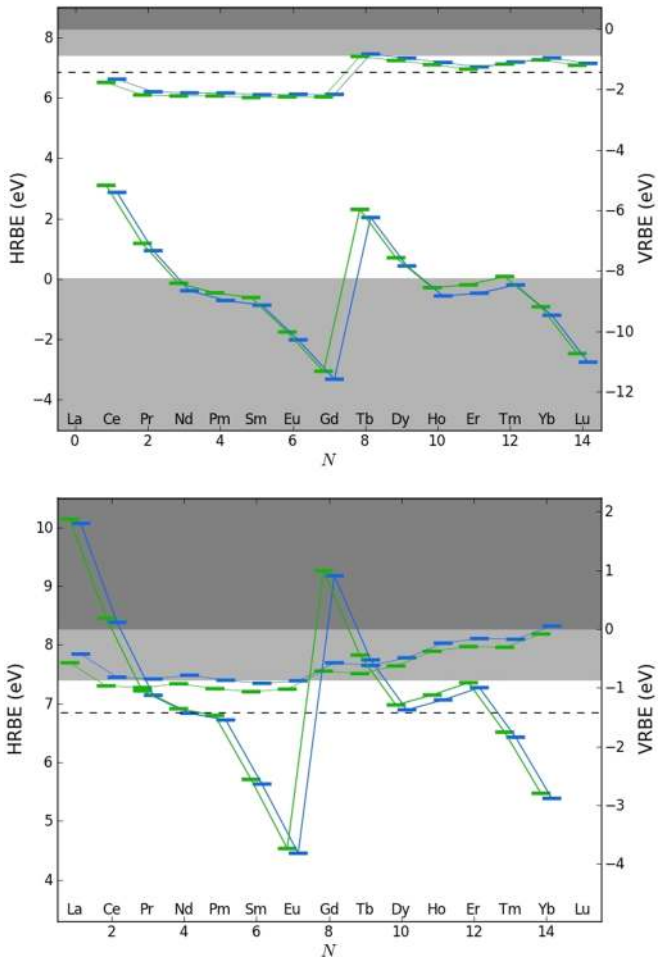

FIG. 9. (Color online) Energy level scheme of the trivalent (top) and divalent (bottom) lanthanides on the Sr1 (green) and Sr2 (blue) sites in monoclinic $SrAl_2O_4$. The zigzag curves display the locations of the $4f^N$ ground states, and the other colored lines the locations of the lowest $4f^{N-1}5d^1$ states. The dashed line represents the lowest excitonic bonding energy, a light-gray background the valence and conduction bands, and a dark-gray background the vacuum.

of the $5d$ electron from the lowest $5d$ level to the conduction band) [31] less thermal energy is needed to quench the blue emission as its (unrelaxed) $5d$ level is considerably closer to the conduction band (Fig. 9).

In Fig. 4(a) both the integrated emission intensity and the luminescence lifetime of the blue emission are plotted as a function of temperature. As can be seen the thermal quenching and luminescence lifetime roughly follow the same trend with a little displacement in temperature of about 50 K. This correlation between thermal quenching and luminescence lifetime can be expected, due to the increased probability of nonradiative decay paths at elevated temperature, thus lowering the emission intensity and reducing the luminescence lifetime values. Many clear examples can be found in literature [32,33].

The thermal quenching behavior of the green emission [Fig. 4(b)] is somewhat more complicated. First of all, the thermal quenching behavior depends on the excitation wavelength which can be seen upon comparison of the main figure and the inset of Fig. 4(b). Upon excitation with 370 nm nearly the same quenching behavior is observed in the 75–275 K temperature range as for the blue emission band. This is not surprising, as the blue emission band shows a significant overlap with the excitation spectrum of the green emission (Fig. 3). Consequently, energy transfer from the blue emitting to the green emitting Eu ions can occur. At temperatures where blue emission is visible, the green emission is comprised of intrinsic green emission (due to absorption by Eu ions on the Sr1 site) and the emission resulting from energy transfer (from Eu ions on the Sr2 site to Eu ions on the Sr1 site). Therefore, as the blue emission quenches upon increasing the temperature up to 300 K, the same quenching behavior is (partially) noticed in the green emission. For temperatures above 300 K the blue emission is completely quenched and the intensity of the remaining green emission band is relatively stable until it starts decreasing around 400 K. Here the "genuine" thermal quenching of the green emission sets in [31], which originates from the ionization related to the distance between the $5d$ level and the bottom of the conduction band (Fig. 9). Considering this anticipated thermal quenching behavior in the high-temperature region, one would expect—when only exciting the green emission center ($\lambda_{ex} = 435$ nm)—that the intensity of the green emission band remains stable up to temperatures around 350 K and only then shows a typical quenching behavior, as depicted by the black dotted curve in Fig. 4(b). However, upon excitation with 435 nm, a limited decrease in emission intensity is observed from temperatures around 220 K [inset of Fig. 4(b)]. The origin of this decrease will be discussed in Sec. IV D.

The complex thermal quenching behavior of the green emission is reflected in the temperature dependency of its luminescence lifetime [Fig. 4(b)]. As described above, at low temperatures the decay of the luminescence is monoexponential with a decay constant of 1140 ns. Above 100 K the decay profile shows two components: a first component for which the lifetime remains stable (1140 ns) upon increasing the temperature and a second, temperature-dependent faster decaying component. For this second component, the higher the temperature, the faster this decay becomes and the larger the fraction it represents in the total emission. The stable decay component is in line with what we would expect when no thermal quenching is present. Since the observed drop in emission intensity around 220 K is presumably a consequence of the trapping processes that start to play a role around that temperature (as will be shown in Sec. IV F), the manifestation of the second fast component might also be related to trapping processes.

C. Charging behavior

In Fig. 5(a) the integrated emission intensity as a function of charging time is plotted, for different charging temperatures. The shape of the curve is very temperature dependent. Below 230 K the integrated emission intensity remains nearly constant during the excitation, while for higher temperatures a monotonic increase of the integrated emission intensity towards an equilibrium value can be observed. The higher the temperature, the faster this increase and the lower the final equilibrium value. The monotonic increasing shape is often

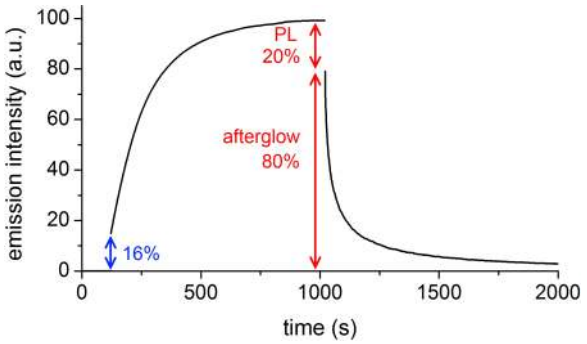

FIG. 10. (Color online) Charging curve ($\lambda_{ex} = 435$ nm) started at $t = 120$ s and afterglow curve started at $t = 1020$ s ($T = 293$ K).

referred to as "charging behavior" of a persistent luminescent phosphor, being the competition between the steady state luminescence and the filling of traps. However, at low temperature where this charging behavior seems absent based on the shape of the emission intensity curve, charging of the phosphor does occur, as a significant TL glow curve is measured afterwards [Fig. 5(c)]. Ascribing the monotonic increasing shape solely to the competition between the (emissive) photoluminescence and the (nonemissive) trap filling of the persistent luminescent phosphor is thus inadequate. What is then the cause of the monotonic increase during the excitation?

The luminescent emission upon excitation of persistent luminescent phosphors is comprised of both regular PL emission and emerging afterglow emission. It is obvious that the afterglow emission does not suddenly start when the excitation source is switched off; it is already present during the excitation. As soon as electrons get trapped at the very start of the excitation they can get detrapped (depending on the thermal energy available) and cause afterglow emission. The trapping of the electrons occurs at a higher rate than the detrapping so there is a fast buildup of the number of filled traps and an associated increase of the afterglow emission. The monotonic increase of the integrated emission intensity during excitation is thus largely related to the increasing afterglow emission. A good measure for the increase in integrated emission intensity being caused by the afterglow is provided by the afterglow emission intensity immediately after switching off the excitation source. This can be seen in Fig. 10, in which the charging curve upon excitation with 435 nm and afterglow curve (at 293 K) are shown. The increase in emission intensity upon charging of the phosphor is indeed comparable to the amount of afterglow emission immediately after switching off the excitation source. It can also be seen that near the end of the excitation, where the charging curve reaches a constant regime, the emission is composed of both PL (20%) and afterglow (80%), with the latter clearly dominating.

This hypothesis on the origin of the monotonically increasing charging curve is also able to explain why at temperatures lower than 235 K the integrated emission intensity remains nearly constant or even slightly decreases during excitation. Although there is trap filling at these low temperatures (witnessed by the TL emission), there is not enough thermal energy to release electrons from their traps during the excitation [cf. the absence of afterglow at these temperatures (Fig. 5(b))]. The decrease of the charging curve, albeit limited, is explained by the reduction in the concentration of divalent Eu ions, as certain Eu^{2+} ions lose their electron towards traps, turning them into Eu^{3+} ions with low absorption strength. As a result, the incoming light will cover a longer path length before absorption, leading to increased scattering losses. In addition, the resulting steady state emission also has a lower chance to effectively leave the phosphor material.

Upon excitation with 435 nm light, the charging curves [Fig. 5(d)] are similar to those in Fig. 5(a) although already for temperatures below 255 K the charging curves show no increase. This implies that at these temperatures there is no afterglow upon excitation with 435 nm, whereas there is afterglow (albeit very limited) upon excitation with 370 nm, hinting at filling of different trap distributions for the two wavelengths.

D. Efficiency of the persistent luminescence

From the inset in Fig. 4 it was seen that upon excitation with 435 nm at a temperature of 293 K the integrated intensity of the green emission band in $SrAl_2O_4$:Eu,Dy is only 70% of the emission intensity at lower temperature (i.e., below 200 K):

$$I_{tot}(293\ \text{K}) = 0.7 I_{tot}(<200\ \text{K}).$$

As the genuine thermal quenching for the green emission only sets in well above 293 K, the deficit in intensity at 293 K must have another origin and can be related to the afterglow process. Indeed, it is reasonable to assume that not every trapped electron will effectively yield radiative recombination at the ionized europium center once it has been thermally released. Consequently, we can define the quantum efficiency of the afterglow process as the number of emitted photons in the afterglow regime divided by the number of trapped charges. From Fig. 10 and the discussion above we know that at 293 K the total emission is comprised of both PL (20%) and afterglow (80%). Because of the very slow heating rate in Fig. 4, it is reasonable to assume that we are constantly in the regime where the charging has reached its maximum value, meaning an equilibrium between trapping and detrapping of electrons. We can thus write for the emission intensity of the steady state luminescence I_{PL} (which does not involve trapping and detrapping) and the afterglow related emission intensity I_{AG}:

$$I_{PL}(293\ \text{K}) = 0.20 I_{tot}(293\ \text{K}) = 0.14 I_{tot}(<200\ \text{K}),$$

$$I_{AG}(293\ \text{K}) = 0.80 I_{tot}(293\ \text{K}) = 0.56 I_{tot}(<200\ \text{K}).$$

Taking into account that the steady state luminescence occurs at the same efficiency at 293 K as at 200 K, as observed from the (luminescence) lifetime remaining constant at 1140 ns, we can now calculate the quantum efficiency of the afterglow process η_{AG} by

$$\eta_{AG}(293\ \text{K}) = \frac{I_{AG}(293\ \text{K})}{I_{tot}(<200\ \text{K}) - I_{PL}(293\ \text{K})} = \frac{0.56}{1 - 0.14} = 0.65.$$

At 293 K, the efficiency of the persistent luminescence is thus about 65% with an estimated error of about 10%, related

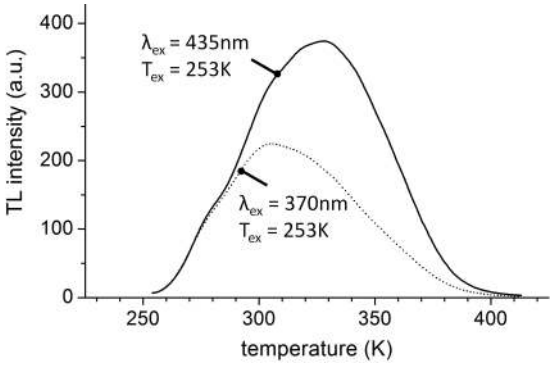

FIG. 11. Thermoluminescence glow curves of $SrAl_2O_4$:Eu,Dy after measuring the afterglow for 30 min at 253 K. Charging was performed for 15 min at 370 (dotted line) or 435 nm (solid line).

to possible errors in the thermal quenching measurement or in deducing the fractions of PL and afterglow. It must be noted that the efficiency of the persistent luminescence might show variation as a function of temperature if other processes, such as thermal quenching, start to play a role. Given that persistent phosphors are commonly used in isothermal conditions (at room temperature), this is an important result for the assessment of the efficiency of a persistent phosphor.

E. Thermoluminescence and afterglow behavior

Figure 11 shows the TL curves of $SrAl_2O_4$:Eu,Dy after 15 min charging and subsequent 30 min afterglow at 253 K using 435 nm light (solid line) and 370 nm light (dotted line) for the charging. Comparing the two TL curves, one can see that they peak at significantly different temperatures: After charging with 435 nm, the TL peak is located at higher temperatures, hence relatively deeper traps are filled than after charging with 370 nm. At the low-temperature side of both TL curves a shoulder at 275 K can be seen. At the temperature where the dotted curve reaches its maximum (305 K) a faint shoulder in the solid curve can be seen. This apparent substructure in the broad TL glow curves clearly hints at the presence of a trap depth distribution in $SrAl_2O_4$:Eu,Dy.

The differences in the TL glow curves after excitation with 370 and 435 nm are also reflected in the afterglow behavior. Comparing the afterglow curves after excitation with these wavelengths [Figs. 5(b) and 5(e)], a few subtle differences were observed. After charging with 370 nm, the initial afterglow intensity (immediately after switching off the excitation source) is a little higher but the decay of the afterglow is much faster when compared to the afterglow intensity when charged with 435 nm. A second difference is noticed at low temperatures ($T < 243$ K): After charging with 370 nm light a faint afterglow can be measured immediately after switching off the excitation source, whereas no afterglow at all can be measured after excitation with 435 nm light. Based on these differences in afterglow behavior, it seems that charging with 370 nm light preferentially fills more shallow traps, while charging with 435 nm light preferentially fills deeper traps. This is in good correspondence with the TL curves. Nevertheless, it appears that in both trap distributions, at least some similar trap depths are encountered.

F. Trapping mechanism

It is clear that the observed differences in charging, afterglow, and TL behavior at different temperatures and upon excitation with different wavelengths (370 and 435 nm) must be related to the trap filling mechanism.

The necessary information on the filling of the traps in $SrAl_2O_4$:Eu,Dy can be deduced from Figs. 6 and 7. Comparing the two figures one can see a few similarities and some striking differences. Let us first discuss the similarities. In both series the amount of afterglow as a function of temperature (blue dots) is very alike: Afterglow arises only if the temperature of the phosphor is at least 250 K; for lower temperatures there is little to no afterglow. This is not unexpected as a certain amount of thermal energy is needed to release electrons from traps. It must be noted that for 243 and 253 K the accumulated afterglow after excitation with 370 nm is a little higher than after excitation with 435 nm, indicating that more shallow traps were filled, which is in line with the observed differences in TL curves (Fig. 11). The major difference between Figs. 6 and 7 is observed in the integrated TL signal as a function of temperature (red triangles). To discuss this difference, we distinguish two temperature regions: the low-temperature region from 193 K up to 223 K and the temperature region from 253 K up to 323 K. In the lower range (and probably for even lower temperatures as well) apparently no traps get filled upon excitation with 435 nm, whereas upon excitation with 370 nm a significant amount of traps get filled. In the higher range the situation is different, as excitation with 435 nm results in significantly more traps being filled (almost twice the amount) than after excitation with 370 nm.

From the above discussion, it is clear that trap filling is thus both dependent on temperature and on the excitation wavelength. For the trapping process, we can discern two steps. During the first stage the $5d$ electron of the excited Eu^{2+} ion needs to be separated from the europium ion. The second step involves the trapping of the (released) electron at a trap level, characterized by a certain depth.

Focusing on the second step, the excitation wavelength determines what traps are finally filled, as the TL glow curves are markedly different for excitation with 435 nm (only exciting the green emitting Eu^{2+} centers) and 370 nm (exciting both blue and green emitting centers), with the most outspoken difference found for the filling of the deeper traps. This immediately proves that a large fraction of the trap centers can only be accessed upon excitation of the green emitting centers. Consequently, (at least part of the) trapping is a local phenomenon, close to the Eu center from which the electron originates. This is an important conclusion, as it shows—by exploiting the fact that two emission centers are present in this material—that a large fraction of the traps are locally coupled to the europium centers. The fact that the TL glow curves coincide on the low-temperature side is not incompatible with this conclusion, as it is possible that the some traps are accessible from both the blue and green emitting centers.

Focusing on the first step of the trapping process, the temperature dependency of the trap filling means that an energy barrier needs to be overcome to transfer an electron from Eu^{2+} to a trap. By means of x-ray absorption techniques, it was indeed shown that an oxidation of europium ions in $SrAl_2O_4$:Eu,Dy occurred during the charging process [34].

This energy barrier is most obvious in the case of excitation with 435 nm, where trap filling occurs only for temperatures above 220 K. In literature, this thermal barrier has been related to the thermal quenching behavior of the steady state luminescence: the higher the thermal quenching behavior, the less likely trap filling occurs upon excitation to the lowest 5*d* states of the Eu^{2+} or Ce^{3+} ions [35–37]. The reasoning is that a higher thermal quenching temperature is related to a larger separation between the 5*d* levels of the lanthanide ion and the bottom of the conduction band. Taking into account the results from the thermal quenching behavior of the blue and green emission center, as well as the results from the energy level modeling, it is more likely to observe a thermal barrier for the trapping in the case of the green emission center.

As thermal quenching of the (green) emission for this excitation wavelength occurs at much higher temperatures ($T > 350$ K) than the trap filling threshold temperature ($T > 220$ K), the thermal energy needed to overcome the energy barrier related to trap filling is considerably less than the thermal energy needed to transfer the electron from the lowest 5*d* level of Eu^{2+} to the conduction band, supposing that this is the mechanism behind thermal quenching [31]. Although it is likely that electron delocalization occurs during the trapping process, it seems that it does not have to imply a full delocalization to the conduction band.

V. CONCLUSIONS

The origin of the green and blue emission bands in $SrAl_2O_4$:Eu,Dy was thoroughly studied and attributed to the incorporation of Eu^{2+} on the two inequivalent Sr sites in the $SrAl_2O_4$ host, based on the emission, excitation, and luminescence lifetime properties of both emission bands. Moreover, it was verified that the difference in spectroscopic redshift for both emission bands can be assigned to the difference in surrounding of the two Sr sites. The large difference in Stokes shift for the two emission bands is more difficult to explain, but it might be related to differences in the angular charge distribution in the first coordination sphere of the Sr1 and Sr2 sites.

Using empirical relations, a complete energy level scheme was constructed for all divalent and trivalent lanthanide ions, incorporated on the Sr1 and Sr2 sites in monoclinic $SrAl_2O_4$. Based on the position of the lowest 5*d* levels for Eu^{2+} incorporated on the two different Sr sites, the difference in thermal quenching of the blue and green emission bands could then easily be understood.

In addition to the well-known temperature dependency of the afterglow in persistent luminescent phosphors, we now show that also the filling of traps in $SrAl_2O_4$:Eu,Dy is temperature dependent. An energy barrier needs to be overcome for the 5*d* electron of excited Eu^{2+} ions to get trapped upon excitation with blue light. Nevertheless, the critical temperature lies well below room temperature, in contrast to other persistent phosphors [35], which does not hamper the common applications. Additionally, a considerable difference in trap filling was shown upon charging $SrAl_2O_4$:Eu,Dy with different wavelengths. Markedly different and deeper traps were filled upon exclusive excitation via the green emitting centers, confirming the local character of the trapping. Consequently, it appears that full delocalization of the liberated electron does not occur, as then trapping could occur far away from the original europium ion, where no distinction would be made between different types of traps (with correspondingly different depths). There still remains strong debate about the chemical nature of the trapping centers. More specifically for $SrAl_2O_4$:Eu,Dy it is not agreed upon whether the Dy^{3+} codopant acts as an electron trap, thereby becoming Dy^{2+} [15–17,38]. Based on the shape of the TL glow curves, it is clear that $SrAl_2O_4$:Eu,Dy contains different trap centers, with different associated trap depths. Clearly, intrinsic defects play a role, judging on the occurrence of afterglow in $SrAl_2O_4$:Eu, without codopants. Based on the energy level scheme for the divalent lanthanides (Fig. 9), the position of the Dy^{2+} ground state is compatible with a trap depth relevant for the occurrence of afterglow emission around room temperature. Depending on the Sr site dysprosium substitutes for, a difference in trap depth of about 0.1 eV is found for Dy^{3+} on both sites. Given the apparently local nature of the trapping, clustering of europium and dysprosium on specific lattice sites could explain the difference in trap depth distribution upon excitation with blue or near-UV light. Obviously, further research is needed to substantiate this hypothesis.

In our experiments, we combined charging, afterglow, and TL measurements in the same run, which for instance allows one to get an absolute comparison between afterglow and TL. Furthermore, it gives an indication about the total number of trapped charges. Using such an integrated approach thus seems an advantageous strategy to gain deeper insight into the trapping and detrapping processes of persistent phosphors. As all three parts in these experiments are manifestations of the same underlying processes (continuous filling and emptying of the trap distribution), the obtained information from the three parts can be combined. Future work will deal with deriving a relevant trap distribution to simultaneously explain all three processes, with the same underlying trap distribution. Combined with assumptions on the trapping and detrapping processes, the derived model should also be able to predict the influence of, for instance, the excitation intensity and the temperature at which the excitation was performed, while using the same model parameters.

For persistent luminescent phosphors, the ability of recording TL glow curves starting below room temperature is a great advantage. For these materials already sufficient thermal energy is available to empty filled traps at room temperature. Therefore, measuring TL glow curves from temperatures well below room temperature is a must to have the correct insight into the entire shape of the TL glow curve and the underlying trap depth distribution. It also explains why, at room temperature, the largest fraction of the emission during excitation is composed of afterglow related emission, for which trapping and detrapping had occurred.

Finally, a method to determine the quantum efficiency of the persistent luminescence was introduced. At 293 K, it turns out that 65% (+/−10%) of the trapped electrons eventually give rise to afterglow emission. Consequently, when using phosphors for color conversion in white LEDs, it seems advantageous to avoid the presence of afterglow, as the process

of trapping and detrapping can be expected to lead to some efficiency losses, compared to direct photoluminescence.

ACKNOWLEDGMENTS

J.B. and J.J.J. are grateful to the Special Research Fund of Ghent University (BOF-UGent) and the agency for Innovation by Science and Technology (IWT) for financial support. The authors would like to thank Katrien Meert and Koen Van den Eeckhout for critical reading and suggestions.

APPENDIX A: CRYSTAL STRUCTURE OF $SrAl_2O_4$

The monoclinic structure of $SrAl_2O_4$ was first described by Schulze and Müller-Buschbaum in 1981 [23]. The structure contains two nonequivalent Sr sites, both having coordination number (CN) 9 and being described by the C_1 point group, as nontrivial symmetry operations are lacking. Bond lengths range from 2.5 to 3.5 Å for both sites. For use in the following discussion, average and effective bond lengths, d_{av} and d_{eff}, respectively, are defined and calculated as follows:

$$\frac{1}{d_{eff}^6} = \frac{1}{CN}\sum_{i=1}^{CN}\frac{1}{[d_i - f(R_M - R_{Ln})]^6}, \quad \text{(A1)}$$

$$d_{av} = \langle d\rangle - f(R_M - R_{Ln}). \quad \text{(A2)}$$

These distances give a measure for the size of the coordination polyhedron, adapted for the relaxation which originates from the substitution of a lanthanide ion on the site of a metal ion with a different ionic radius, R_{Ln} and R_M, respectively. $\langle d\rangle$ is the arithmetic average of the bond lengths in the undoped crystal. The constant f measures the strength of the lattice relaxation and is typically chosen in the range of 0.5–0.7. Here $f = 0.6$ was taken, and $R_{Sr2+} = 1.32$ Å and $R_{Eu2+} = 1.31$ Å were used [23,39]. Crystallographic data on the two Sr sites are summarized in Table II [40–42].

APPENDIX B: SPECTROSCOPIC PARAMETERS FOR $SrAl_2O_4$:Eu^{2+}

The redshift $D(Eu^{2+},A)$ in a compound A is the result of two effects: (i) a lowering of the average of the $4f^65d$ levels with respect to the location in the free ion [the centroid shift, $\epsilon_c(Eu^{2+},A)$] and (ii) a splitting of the $4f^65d$ levels due to the lowering of the symmetry by the incorporation into the crystal [the crystal field splitting $\epsilon_{cfs}(Eu^{2+},A)$] [28]:

$$D(Eu^{2+},A) = \epsilon_c(Eu^{2+},A) - \Delta\epsilon_c(Eu^{2+},\text{free}) + \frac{\epsilon_{cfs}(Eu^{2+},A)}{r(Eu^{2+},A)} + \Delta\epsilon_{cfs}(Eu^{2+},\text{free}). \quad \text{(B1)}$$

In Eq. (B1), $1/r(Eu^{2+},A)$ is the fraction of the crystal field splitting contributing to the redshift, $\Delta\epsilon_c(Eu^{2+},\text{free})$ is the location of the $4f^65d$ barycenter with respect to the lowest $4f^65d$ level in the free Eu^{2+} ion, and $\Delta\epsilon_{cfs}(Eu^{2+},\text{free})$ is the part of the remaining splitting of the underlying $4f^6(^7F)$ term that contributes to the redshift [43]. Usually, $\Delta\epsilon_{cfs}(Eu^{2+},\text{free})$ is approximated by using the energy level scheme of Eu^{3+}. From the degeneracy weighted average of the Eu^{3+} $4f^6(^7F_J)$ multiplets, a value of $\Delta\epsilon_{cfs}(Eu^{2+},\text{free}) = 0.39$ eV is obtained [43,44].

The redshift values of both excitation spectra were determined by taking the point where the intensity equals 20% of the first maximum of the overlapping staircase structure which originates from the splitting of the underlying $4f^6(^7F)$ term. This yields a good estimate of the location of the lowest $4f^6(^7F_0)$ level [43,45].

Obtaining accurate experimental values for the $5d$ crystal field splitting of Eu^{2+} is a tedious undertaking for low coordination symmetries. In this particular case, the $4f^65d^1$ level is split by the crystal field into five bands which strongly overlap due to the energy level structure of the remaining $4f^6$ configuration. Hence, a broad and relatively featureless band is obtained, which is, for instance, in contrast to the case of Ce^{3+}, having only a single $4f$ electron in the ground state [32]. In the case of $SrAl_2O_4$:Eu^{2+}, an estimate of the crystal field splitting can nevertheless be made since fundamental absorption only becomes significant at 6.50 eV and therefore does not appear in the part of the excitation spectrum that is related to $4f^7 \rightarrow 4f^65d^1$ absorption due to the Eu^{2+} impurities [46]. In analogy with the low energy side, the point where the intensity is 20% of the maximum of the staircase structure is selected to pin the highest $4f^6(^7F_6)$ level. By subtracting both values, an energy difference is obtained which equals the crystal field splitting combined with the total splitting energy of one $4f^6(^7F)$ term. This can be accurately approximated by using the splitting energy of the $4f^6(^7F)$ term in Eu^{3+}, being 0.62 eV [43,44].

Once the experimental redshift and crystal field splitting are determined, the experimental centroid shifts can also be calculated with Eq. (B1). A value of $\Delta\epsilon_c(Eu^{2+},\text{free}) = 1.12$ eV was used, based on the energy scheme constructed by Sugar and Spector [28,47]. It can be assumed that $r(Eu^{2+},A)$ is equal for both lattice sites. A point charge model was applied to verify this [48]. $r(Eu^{2+},A) = 1/0.45$ was obtained for both Sr sites within this model. The experimental values for $\epsilon_c(Eu^{2+},A)$ are included in Table I. The experimental ratios are

$$\frac{\epsilon_{cfs}(\text{green})}{\epsilon_{cfs}(\text{blue})} = 0.97 \quad \text{and} \quad \frac{\epsilon_c(\text{green})}{\epsilon_c(\text{blue})} = 1.14. \quad \text{(B2)}$$

Both the centroid shift and the crystal field splitting can be related to the size and nature of the coordination polyhedral

TABLE II. Effective and average bond lengths [as defined in Eqs. (A1) and (A2)], arithmetic average of the bond lengths, and polyhedral volume V of the Sr sites in $SrAl_2O_4$:Eu^{2+}.

	Sr1	Sr2
d_{eff} (Å)	2.741	2.830
d_{av} (Å)	2.872	2.718
$\langle d\rangle$ (Å)	2.878	2.836
V (Å^3)	41.52	40.04

by (semi-) empirical formulas:

$$\frac{\epsilon_c}{\mathrm{CN}} = \frac{\alpha_{\mathrm{sp}} e^2}{4\pi\epsilon_0 d_{\mathrm{eff}}^6}(\langle\psi_{5\mathrm{d}}|r^2|\psi_{5\mathrm{d}}\rangle - \langle\psi_{4\mathrm{f}}|r^2|\psi_{4\mathrm{f}}\rangle) \tag{B3}$$

and

$$\epsilon_{\mathrm{cfs}} = \frac{\beta_{\mathrm{poly}}^Q}{d_{\mathrm{av}}^2}. \tag{B4}$$

In these expressions, α_{sp} and β_{poly}^Q are empirical parameters, introduced by Dorenbos [49,50].

Equation (B3) was originally introduced for Ce^{3+}, but the theoretical basis for this empirical relation is more generally valid for $4f^N5d^1$ configurations as was derived by Morrison, based on a suggestion of Judd [50,51].

From the crystallographic data of $SrAl_2O_4$ (Table II) and the above algebra, it can now be verified whether it is plausible that the two different redshifts originate from incorporation of Eu^{2+} on the Sr1 and Sr2 sites. For this, the assumption is made that α_{sp}, β_{poly}^Q, and the expectation values $\langle r^2\rangle$ are equal for both lattice sites and the difference in redshift is thus the mere consequence of the difference in bond length. This yields

$$\frac{\epsilon_{\mathrm{cfs}}(\mathrm{Sr1})}{\epsilon_{\mathrm{cfs}}(\mathrm{Sr2})} = \frac{d_{\mathrm{av}}^2(\mathrm{Sr2})}{d_{\mathrm{av}}^2(\mathrm{Sr1})} = 0.90 \quad \text{and}$$
$$\frac{\epsilon_{\mathrm{c}}(\mathrm{Sr1})}{\epsilon_{\mathrm{c}}(\mathrm{Sr2})} = \frac{d_{\mathrm{eff}}^6(\mathrm{Sr2})}{d_{\mathrm{eff}}^6(\mathrm{Sr1})} = 1.21. \tag{B5}$$

Regardless the simplicity of the model, these calculated ratios are in good correspondence (deviations of only 0.07 and 0.06) with the experimental ratios for the green and blue emission bands. Therefore, it is certainly plausible that the different spectral features are the consequence of the small but significant difference between the two lattice sites. The green emission band is attributed to the Sr1 site, and the blue emission to the Sr2 site. The obtained energy level scheme is displayed in Fig. 8. Herein, the relative locations of the five $4f^6 5d^1$ levels after crystal field splitting were estimated with a point charge model [48]. A good qualitative correspondence with the experimental spectrum is observed, when adding up all the different sublevels. Represented in this way, it is also clear that upon excitation into higher excited levels, the multitude of sublevels leads to a quick relaxation to the lowest excited state, even at low temperature. Hence, the hypothesis that the blue emission originates from emission starting at higher excited states can be discarded. In addition, the clear differences on the high energy side of the excitation spectrum point at a different origin of both emission bands as well.

APPENDIX C: ENERGY LEVEL SCHEMES FOR LANTHANIDES IN $SrAl_2O_4$

The goal is to construct a complete energy level scheme for all divalent and trivalent lanthanide ions on the Sr1 and Sr2 sites of $SrAl_2O_4$. This is done in the framework of the chemical shift model [52]. The chemical shift of a lanthanide ion is defined as the difference in vacuum referred binding energy (VRBE) of the ion in the host material and in free space. The chemical shifts for Eu^{2+} and Eu^{3+} are crucial quantities and can be calculated in an indirect way. In this model, the Coulomb repulsion $U(\mathrm{Eu}, A)$ for europium is introduced, being the distance in energy space between the $4f^N$ ground states of Eu^{2+} and Eu^{3+} in a certain compound A. An empirical relationship was recently established to calculate this Coulomb repulsion from the centroid shift of Ce^{3+} [53]:

$$U(\mathrm{Eu}, A) = 5.44 + 2.834e^{-\epsilon_c(\mathrm{Ce}^{3+}, A)/2.2}. \tag{C1}$$

From U, the chemical shifts for europium are obtained [52]:

$$E_{4\mathrm{f}}^{\mathrm{chem}}(\mathrm{Eu}^{2+}, A) = \frac{U(\mathrm{Eu,free}) - U(\mathrm{Eu}, A)}{0.777 - 0.0353U(\mathrm{Eu}, A)}, \tag{C2}$$

$$E_{4f}^{\mathrm{chem}}(\mathrm{Eu}^{3+}, A) = E_{4f}^{\mathrm{chem}}(\mathrm{Eu}^{2+}, A) - U(\mathrm{Eu}, A). \tag{C3}$$

The numbers in the denominator are empirical parameters. To determine U(Eu,A), the centroid shift of Ce^{3+} in the same compound should be known. The luminescence of Ce^{3+} in $SrAl_2O_4$ was described by Jia [54]. In the PL emission and excitation spectra, two clearly different features were observed and ascribed to incorporation of Ce^{3+} on the two different Sr sites in $SrAl_2O_4$. Analogous to the Eu^{2+} case, the spectral component with the largest redshift is assigned to the Sr1 site. This component shows the smallest crystal field splitting and the largest centroid shift, as in the Eu^{2+} case. The derived values for the centroid shift are then 2.65 and 2.23 eV, for Ce^{3+} on the Sr1 and Sr2 sites, respectively, and can be used to calculate the chemical shifts.

There are two possibilities to construct the so-called zigzag curves in the energy level schemes, representing the ground state energies for the divalent and trivalent rare earth ions. One could use the values of $\overline{\Delta E(\mathrm{Ln,Eu}, Q)}$, reported at multiple places, for example in Ref. [42]. These values define the energy difference of the binding energies of the $4f^N$ ground states for the lanthanide ions (charge Q), with respect to the $4f^N$ ground state of europium. These values represent mean values, obtained from a multitude of host materials. Another possibility stems from the chemical shift model, in which a relationship is established between the chemical shift and the contraction tilt parameter. This contraction tilt parameter allows one to calculate the energy differences $\Delta E(\mathrm{Ln,Eu}, Q)$ which are specific for a certain host material (or more correct, for a certain lattice site). For more details, we refer to Ref. [52].

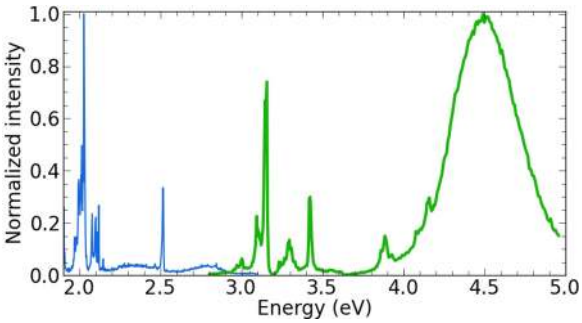

FIG. 12. (Color online) Photoluminescence emission (thin blue line) and excitation spectrum (thick green line) of $SrAl_2O_4$:Eu^{3+} at 10 K. The emission spectrum was measured upon excitation at 275 nm. The excitation spectrum was obtained upon monitoring the emission at 611 nm.

Now, the VRBEs of the divalent and trivalent lanthanides are available. In order to relate this to the valence (VB) and conduction bands (CB) of the host, additional information is necessary. Most often, the location of a charge transfer (CT) band of a trivalent lanthanide is used to probe the distance between the top of the valence band and the $4f^N$ ground state of the divalent lanthanide [55]. In this specific case, we have two nonequivalent optical centers in the same host. Therefore, VB and CB should for both calculations be located in the same position with respect to the vacuum. This condition pins, in turn, the difference in CT energies for the Ln^{3+} on the Sr1 and Sr2 sites. If Eu^{3+} is considered, the energy difference is calculated to be 0.08 eV.

In $SrAl_2O_4$:Eu^{3+}, only one CT band is observed, peaking at 276 nm (4.49 eV) (Fig. 12). It is expected that this broadband is composed of the two components, as calculated above, albeit with a small energy difference of 80 meV, corresponding to 5 nm at 276 nm. Due to the intrinsic high widths of CT bands, this seemingly leads to a single CT band in the experimental spectrum. Consequently, the ground states of Eu^{2+} are found to be 4.53 eV (for Sr1) and 4.45 eV (for Sr2) above the top of the valence band. Finally, the energy level scheme can be completed by merging all calculated values, and taking the band gap of $SrAl_2O_4$ into account [46,56].

[1] K. Van den Eeckhout, P. F. Smet, and D. Poelman, Materials **3**, 2536 (2010).
[2] T. Matsuzawa, Y. Aoki, N. Takeuchi, and Y. Murayama, J. Electrochem. Soc. **143**, 2670 (1996).
[3] Y. Murayam, N. Takeuchi, Y. Aoki, and T. Matsuzawa, Patent No. EP0622440 (1994).
[4] K. Van den Eeckhout, D. Poelman, and P. F. Smet, Materials **6**, 2789 (2013).
[5] Q. le Masne de Chermont, C. Chanéac, J. Seguin, F. Pellé, S. Maîtrejean, J.-P. Jolivet, D. Gourier, M. Bessodes, and D. Scherman, Proc. Natl. Acad. Sci. USA **104**, 9266 (2007).
[6] T. Maldiney, G. Sraiki, B. Viana, D. Gourier, C. Richard, D. Scherman, M. Bessodes, K. Van den Eeckhout, D. Poelman, and P. F. Smet, Opt. Mater. Express **2**, 261 (2012).
[7] M. Sun, Z.-J. Li, C.-L. Liu, H.-X. Fu, J.-S. Shen, and H.-W. Zhang, J. Lumin. **145**, 838 (2014).
[8] B. P. Chandra, J. Lumin. **131**, 1203 (2011).
[9] V. K. Chandra and B. P. Chandra, Opt. Mater. **34**, 194 (2011).
[10] C. N. Xu, T. Watanabe, M. Akiyama, and X. G. Zheng, Appl. Phys. Lett. **74**, 2414 (1999).
[11] C. N. Xu, H. Yamada, X. Wang, and X.-G. Zheng, Appl. Phys. Lett. **84**, 3040 (2004).
[12] Y. Jia, M. Yei, and W. Y. Jia, Opt. Mater. **28**, 974 (2006).
[13] F. C. Palilla, A. K. Levine, and M. R. Tomkus, J. Electrochem. Soc. **115**, 642 (1968).
[14] A. Nag and T. R. N. Kutty, J. Alloy. Compd. **354**, 221 (2003).
[15] P. Dorenbos, J. Electrochem. Soc. **152**, H107 (2005).
[16] F. Clabau, X. Rocquefelte, S. Jobic, P. Deniard, M. H. Whangbo, A. Garcia, and T. Le Mercier, Chem. Mater. **17**, 3904 (2005).
[17] T. Aitasalo, J. Hölsä, H. Jungner, J.-C. Krupa, M. Lastusaari, J. Legendziewicz, and J. Niittykoski, Radiat. Meas. **38**, 727 (2004).
[18] P. Dorenbos, A. J. J. Bos, N. R. J. Poolton, and F. T. You, J. Lumin. **133**, 45 (2013).
[19] A. Vedda, M. Martini, F. Meinardi, J. Chval, M. Dusek, J. Mares, E. Mihokova, and M. Nikl, Phys. Rev. B **61**, 8081 (2000).
[20] T. Maldiney *et al.*, Nat. Mater. **13**, 418 (2014).
[21] L. Chen, Y. Zhang, F. Liu, A. Luo, Z. Chen, Y. Jiang, S. Chen, and R.-S. Liu, Mater. Res. Bull. **47**, 4071 (2012).
[22] C.-W. Yeh, Y. Li, J. Wang, and R.-S. Liu, Opt. Express **20**, 18031 (2012).
[23] A. R. Schulze and H. M. Buschbaum, Z. Anorg. Allg. Chem. **475**, 205 (1981).
[24] G. Blasse and A. Bril, Philips Res. Rep. **23**, 201 (1968).
[25] G. Blasse, W. L. Wanmaker, and J. W. ter Vrugt, J. Electrochem. Soc. **115**, 673 (1968).
[26] S. H. M. Poort, W. P. Blokpoel, and G. Blasse, Chem. Mater. **7**, 1547 (1995).
[27] J. Hölsä, T. Laamanen, M. Lastusaari, M. Malkamäki, and P. Novák, Photon Science 2009, Deutsches Elektronen-Synchrotron Highlights and Hasylab Annual Report, 2009, p. 91.
[28] P. Dorenbos, J. Phys.: Condens. Matter **15**, 4797 (2003).
[29] P. Dorenbos, Chem. Mater. **17**, 6452 (2005).
[30] N. Avci, K. Korthout, M. A. Newton, P. F. Smet, and D. Poelman, Opt. Mater. Express **2**, 321 (2012).
[31] P. Dorenbos, J. Phys.: Condens. Matter **17**, 8103 (2005).
[32] V. Bachmann, C. Ronda, and A. Meijerink, Chem. Mater. **21**, 2077 (2009).
[33] V. Bachmann, C. Ronda, O. Oeckler, W. Schnick, and A. Meijerink, Chem. Mater. **21**, 316 (2009).
[34] K. Korthout, K. Van den Eeckhout, J. Botterman, S. Nikitenko, D. Poelman, and P. F. Smet, Phys. Rev. B **84**, 085140 (2011).
[35] P. F. Smet, K. Van den Eeckhout, A. J. J. Bos, E. van der Kolk, and P. Dorenbos, J. Lumin. **132**, 682 (2012).
[36] E. van der Kolk, S. A. Basun, G. F. Imbusch, and W. M. Yen, Appl. Phys. Lett. **83**, 1740 (2003).
[37] E. van der Kolk, P. Dorenbos, C. W. E. van Eijk, S. A. Basun, G. F. Imbusch, and W. M. Yen, Phys. Rev. B **71**, 165120 (2005).
[38] M. Lastusaari, H. F. Brito, S. Carlson, J. Holsa, T. Laamanen, L. C. V. Rodrigues, and E. Welter, Phys. Scr. **89**, 044004 (2014).
[39] G. Giraud *et al.*, Int. J. Mol. Sci. **10**, 1930 (2009).
[40] P. Dorenbos, Phys. Rev. B **65**, 235110 (2002).
[41] P. Dorenbos, J. Phys.: Condens. Matter **15**, 2645 (2003).
[42] P. Dorenbos, Phys. Rev. B **62**, 15640 (2000).
[43] P. Dorenbos, J. Phys.: Condens. Matter **15**, 575 (2003).
[44] W. T. Carnall, P. R. Fields, and K. Rajnak, J. Chem. Phys. **49**, 4450 (1968).
[45] P. Dorenbos, J. Lumin. **104**, 239 (2003).
[46] M. Kamada, J. Murakami, and N. Ohno, J. Lumin. **87-89**, 1042 (2000).
[47] J. Sugar and N. Spector, J. Opt. Soc. Am. **64**, 1484 (1974).
[48] S. Sugano, Y. Tanabe, and H. Kamimura, *Multiplets of Transition Metal Ions in Crystals* (Academic, New York, 1970).

[49] P. Dorenbos, J. Alloy. Compd. **341**, 156 (2002).
[50] P. Dorenbos, J. Andriessen, and C. W. E. van Eijk, J. Solid State Chem. **171**, 133 (2003).
[51] C. A. Morrison, J. Chem. Phys. **72**, 1001 (1980).
[52] P. Dorenbos, Phys. Rev. B **85**, 165107 (2012).
[53] P. Dorenbos, J. Lumin. **135**, 93 (2013).
[54] D. Jia, J. Lumin. **117**, 170 (2006).
[55] P. Dorenbos, J. Phys.: Condens. Matter **15**, 8417 (2003).
[56] J. Hölsä, T. Laamanen, M. Lastusaari, J. Niittykoski, and P. Novák, J. Rare Earths **27**, 550 (2009).